

The Kibble-Zurek Scenario and Coarsening Across Nonequilibrium Phase Transitions in Driven Vortices and Skyrmions

C. Reichhardt and C. J. O. Reichhardt

*Theoretical Division and Center for Nonlinear Studies,
Los Alamos National Laboratory, Los Alamos, New Mexico 87545, USA*

(Dated: July 7, 2023)

We investigate the topological defect populations for superconducting vortices and magnetic skyrmions on random pinning substrates under driving amplitudes that are swept at different rates or suddenly quenched. When the substrate pinning is sufficiently strong, the system exhibits a nonequilibrium phase transition at a critical drive into a more topologically ordered state. We examine the number of topological defects that remain as we cross the ordering transition at different rates. In the vortex case, the system dynamically orders into a moving smectic, and the Kibble-Zurek scaling hypothesis gives exponents consistent with directed percolation. Due to their strong Magnus force, the skyrmions dynamically order into an isotropic crystal, producing different Kibble-Zurek scaling exponents that are more consistent with coarsening. We argue that in the skyrmion crystal, the topological defects can both climb and glide, facilitating coarsening, whereas in the vortex smectic state, the defects cannot climb and coarsening is suppressed. We also examine pulsed driving across the ordering transition and find that the defect population on the ordered side of the transition decreases with time as a power law, indicating that coarsening can occur across nonequilibrium phase transitions. Our results should be general to a wide class of nonequilibrium systems driven over random disorder where there are well-defined topological defects.

I. INTRODUCTION

Phase transitions, such as the transition from solid to fluid or the change from paramagnetic to ferromagnetic, are well studied in equilibrium systems, and may have discontinuous first-order character or continuous second-order character^{1,2}. Typically these transitions are identified via an order parameter, symmetry breaking, or the formation of topological defects. There has been growing interest in understanding whether nonequilibrium systems can also exhibit phase transition behavior, and if so, how this behavior can be characterized³. There are now several systems that have shown strong evidence for nonequilibrium phase transitions, such as transitions among different turbulent states⁴⁻⁷, reorganization of periodically sheared colloidal systems⁸, and emergent behaviors in systems with non-reciprocal interactions⁹.

Another phenomenon exhibiting behavior consistent with a nonequilibrium phase transition is the depinning of particles coupled to random or disordered substrates¹⁰⁻¹². For example, the depinning of elastic objects such as charge density waves from a random substrate shows scaling near the depinning threshold^{10,12}. Other models with strong plasticity, such as the depinning of colloidal particles or vortices in type-II superconductors, also exhibit scaling of the velocity-force curves near depinning with different exponents than those found for elastic depinning^{11,12}. A wide variety of continuous and first-order behavior can occur during depinning from ordered substrates due to the formation of kinks or solitons that can produce hysteresis across the transition, indicative of the type of metastability associated with a first-order transition¹²⁻¹⁴. One of the most studied depinning systems is vortices in type-II superconductors, which in the absence of quenched disorder form a tri-

angular lattice¹⁵. When the underlying disordered substrate is strong enough, the vortices form a topologically disordered state that can undergo plastic depinning, and at higher drives there is a dynamical ordering transition into a moving smectic or anisotropic crystal¹⁶⁻²⁵. Above the ordering transition, a large fraction of the vortices have six neighbors as in a perfect lattice, but a moving isotropic crystal does not form due to the anisotropic fluctuations produced by the pinning on the moving vortex structure. In two-dimensional (2D) systems, the strongly driven vortices organize into a smectic state consisting of a series of chains of vortices that slide past each other. In this case, there can still be several topological defects present in the form of dislocations composed of pairs of fivefold and sevenfold disclinations (5-7 pairs) that slide in the direction of drive, so that in the dynamically re-ordered state, the Burger's vectors of all of the dislocations are oriented along the same direction.

The dynamical ordering of vortices at high drives has been studied with neutron scattering and direct imaging^{18,23}, but it can also be deduced from features in the velocity-force curves and peaks in the differential conductivity^{16,19,24}. When thermal fluctuations are important, the vortices can still dynamically order at higher drives but the driving force needed to order the system diverges as the temperature T approaches the pin-free melting temperature^{17,19}. The dynamical ordering can also produce signatures in the conduction noise. Near depinning, the noise has a strong $1/f^\alpha$ signature and there is a large amount of low frequency noise power, while above the dynamical reordering transition, the noise has narrow band characteristics and the noise power is low^{24,26,27}. Similar dynamical ordering of particle-like systems has also been studied for colloids²⁸, Wigner crystals^{29,30}, pattern forming

systems^{31,32}, frictional systems³³, active matter³⁴, and magnetic skyrmions^{35–37}.

Recently it was shown in simulations and experiments that dynamical ordering transitions in driven vortices and colloids can also be examined within the framework of the Kibble-Zurek (KZ) scenario^{38,39}. Under equilibrium conditions, when a phase transition occurs from a disordered to an ordered phase as a function of some control parameter, there can be well-defined topological defects such as domain walls, dislocations, or, in the case of superfluid transitions, vortices. If the control parameter is changed slowly so that the system remains in the adiabatic limit, topological defects will be absent on the ordered side of the transition. According to the KZ scenario, however, if the control parameter is swept across the transition sufficiently rapidly, topological defects persist on the ordered side of the transition, and the defect density P_d scales as a power law $P_d \propto \tau_q^{-\beta}$, where τ_q is the time duration of the quench of the control parameter across the transition^{40–43}. The exponent β is related to the universality class and scaling of the underlying second order phase transition according to $\beta = (D-d)\nu/(1+z\nu)$, where D is the dimension of the system, d is the dimension of the defects, and z and ν are the critical exponents that relate to the specific universality class of the transition. The KZ scenario has been studied in a variety of equilibrium systems such as liquid crystals⁴⁴, superfluid vortices⁴⁵, ion crystals^{46,47}, 2D colloidal systems⁴⁸ and cold atoms⁴⁹.

In principle, the KZ scenario can be applied to nonequilibrium phase transitions when well-defined topological defects can be identified. There have been some applications of the KZ scenario to nonequilibrium systems for which the underlying phase transition is in an equilibrium universality class^{50,51}; however, there are other examples of nonequilibrium phase transitions that have no equilibrium counterpart, such as directed percolation^{3,4,7,8}. Recently Reichhardt and Reichhardt studied the defect populations across the dynamical ordering transition of 2D driven superconducting vortices for increasing drive sweep rates $1/\tau_q$, and found power law scaling consistent with the KZ scenario³⁸. Interestingly, the exponents in the vortex system were consistent with 1 + 1-dimensional directed percolation³ rather than with the 2D Ising model. Directed percolation is a universality class that is associated with many of the previously observed nonequilibrium phase transitions^{3,4,7,8}. In the case of driven superconducting vortices, the ordered state consists of one-dimensional (1D) chains forming a moving smectic configuration, so it is natural for the system to behave more like a 1D than a 2D system. In Ref.³⁸ it was also shown that colloidal particles driven over quenched disorder form a moving smectic as well, producing the same KZ scaling. Maegochi *et al.* observed similar exponents in an experimental realization of the superconducting vortex system³⁹.

Some of the next questions to address for driven systems are whether the KZ scenario can also be applied in

cases where moving ordered crystals form instead of moving smectics, so that the ordered dynamics are fully 2D. In this case, it would be interesting to determine whether the system would fall into the class of 2D directed percolation, or into some different universality class. Another general question is the possible role of coarsening in these systems. In the case of an instantaneous quench across the ordering transition, there will be a specific defect population, but it is not known if these defects coarsen on the ordered side of the transition even in systems with no thermal fluctuations. In equilibrium systems, when an instantaneous quench is performed from the disordered to the ordered phase, the defect population can exhibit coarsening with different types of power law behaviors that depend on the nature of the defects^{52–55}. Numerical studies of quenches in spin ices also showed that coarsening dominates over the KZ scaling if the topological defects interact sufficiently strongly with each other on the ordered side of the transition⁵⁶.

In this work, we consider both continuous driving and instantaneous quenching across dynamical ordering transitions for superconducting vortices and magnetic skyrmions in two-dimensional systems with quenched disorder. The skyrmions are magnetic particle-like textures^{57–61} that have many similarities to vortices in type-II superconductors in that they form a triangular lattice^{57,58}, can interact with pinning⁶¹, and can be set into motion with an applied drive^{59–66}. There have been several numerical and experimental studies that have demonstrated the dynamical ordering of skyrmions into a crystal under an applied drive^{35–37,67,68}. One of the key differences between skyrmions and superconducting vortices is that skyrmions have a strong Magnus force that creates velocities that are perpendicular to the forces experienced by the skyrmions. As a result, under a drive skyrmions move at an angle with respect to the driving direction, called the skyrmion Hall angle^{35,37,59,67,69–73}. Additionally, the Magnus force affects the fluctuations skyrmions experience from moving over the pinning landscape⁷⁴. In the case of superconducting vortices where the overdamped dynamics cause the velocities to be aligned with the direction of drive, the fluctuations produced by pinning are strongest in the direction of motion, causing the vortices to adopt a smectic configuration; however, for skyrmions, the Magnus forces mix the fluctuations so that they are both parallel and perpendicular to the direction of motion, permitting the skyrmions to form an isotropic lattice^{35,74}. As a result, the moving ordered state is significantly different in the skyrmion and superconducting vortex systems, so an open question is whether the KZ scenario still applies to driven skyrmions, and if so, whether it would fall in a different universality class from that of the vortices. In principle, one would not expect the skyrmions to be in the 1D directed percolation universality class since the ordering of the skyrmion lattice is strongly two-dimensional in character.

Here we show that the skyrmions form a lattice or

polycrystalline crystal rather than a moving smectic and can reach a higher level of dynamical ordering than the superconducting vortices. As a function of the quench time τ_q , the skyrmion defect populations obey a power law scaling with $P_d \propto \tau_q^{-\beta}$, where the observed value of $\beta = 0.5$ is different from the values $\beta = 0.401$ expected for 1D directed percolation and $\beta = 0.64$ expected for 2D directed percolation. We argue that the exponents are consistent with a coarsening process that, in 2D, is expected to give $\beta = 1/2$, indicating that the behavior is more like that of systems with strongly interacting defects subjected to a quench⁵⁶. Once the superconducting vortices form moving 1D channels, the defects are locked into the channels and are unable to climb, so the defect density remains static in the smectic phase. Skyrmions form an isotropic 2D lattice in which the topological defects can both climb and glide. This permits defect annihilation to occur and causes coarsening dynamics to dominate the slow quenches. We cannot rule out the possibility that the skyrmions simply fall into a different universality class of phase transitions than the superconducting vortices; however, we can directly observe coarsening dynamics on the ordered side of the transition by considering instantaneous quenches of the skyrmion system. These quenches reveal that the defect annihilation has a power law dependence on time that is consistent with coarsening to a more ordered state. The instantaneously quenched skyrmion system forms a polycrystalline arrangement rather than the smectic structure observed for superconducting vortices. The coarsening of the skyrmion lattice is most prominent just above the drive where the ordering transition occurs, while at drives much higher than the ordering transition, it occurs in two stages. The first stage consists of the annihilation of individual defects, while the second stage involves the coarsening of the grain boundaries. In the instantaneous quenches, the system can better order closer to the critical points since the effective shaking temperature produced from collisions of the particles with the pinning sites is largest close to the transition, causing the defects to be more mobile.

II. SIMULATION

We consider particle-based models of both superconducting vortices and magnetic skyrmions driven over a random substrate in a two-dimensional system of size $L \times L$ with $L = 36$ and periodic boundary conditions. In both cases, the particles have repulsive interactions modeled as a Bessel function^{61,75}. Throughout this work the sample contains $N_v = 1296$ particles. The skyrmion motion is obtained with a modified Thiele equation that has been used extensively to study collective skyrmion transport effects^{35,61,67,74-77}. The dynamics of a single skyrmion or vortex are given by the following equation of motion:

$$\alpha_d \mathbf{v}_i + \alpha_m \hat{z} \times \mathbf{v}_i = \mathbf{F}_i^{ss} + \mathbf{F}_i^{sp} + \mathbf{F}^D + \mathbf{F}_i^T. \quad (1)$$

The particle velocity is $\mathbf{v}_i = d\mathbf{r}_i/dt$ and dissipation arises from the damping term α_d that aligns the velocity in the direction of the net applied force. The second term on the left is a Magnus force of magnitude α_m that creates a velocity component perpendicular to the net applied forces. One way to characterize the relative importance of the Magnus and damping terms is with the intrinsic skyrmion Hall angle, $\theta_{sk}^{\text{int}} = \arctan(\alpha_m/\alpha_d)$. Skyrmion Hall angles ranging from $\theta_{sk} = 5^\circ$ to 50° have been measured; however, it is likely that larger skyrmion Hall angles are possible in samples containing smaller skyrmions where direct imaging of the skyrmion dynamics is difficult. We fix $\alpha_m^2 + \alpha_d^2 = 1$, and for the vortices, $\alpha_m = 0$ and $\alpha_d = 1$. The skyrmions and vortices have repulsive interactions described by $\mathbf{F}_i^{ss} = \sum_{j=1}^N A_s K_1(r_{ij}) \hat{\mathbf{r}}_{ij}$, where $r_{ij} = |\mathbf{r}_i - \mathbf{r}_j|$ is the distance between particles i and j , $\hat{\mathbf{r}}_{ij} = (\mathbf{r}_i - \mathbf{r}_j)/r_{ij}$, and $K_1(r)$ is the first order Bessel function, which decays exponentially at long range. Experimental evidence exists for repulsive skyrmion interactions that decay exponentially at longer range⁷⁸. The particles also interact with random disorder from the substrate modeled as N_p non-overlapping pinning sites in the form of finite range attractive parabolic wells, with a maximum strength of F_p and a range of $R_p = 0.35$. Here, $\mathbf{F}_i^{sp} = \sum_{k=1}^{N_p} (F_p/R_p) \Theta(\mathbf{r}_{ik}^{(p)} - R_p) \hat{\mathbf{r}}_{ik}^{(p)}$, where the distance between particle i and pin k is $\mathbf{r}_{ik}^{(p)} = \mathbf{r}_i - \mathbf{r}_k$, $\hat{\mathbf{r}}_{ik}^{(p)} = (\mathbf{r}_i - \mathbf{r}_k)/|\mathbf{r}_{ik}^{(p)}|$, and Θ is the Heaviside step function. This model was shown in previous work to capture a variety of vortex and skyrmion behaviors observed in experiment, including dynamic ordering and the velocity dependence of the skyrmion Hall angle. We fix $N_v/N_p = 2$.

The initial particle positions are obtained using simulated annealing with a nonzero temperature represented by Langevin kicks \mathbf{F}_i^T , where $\langle \mathbf{F}_i^T \rangle = 0$ and $\langle \mathbf{F}_i^T(t) \mathbf{F}_j^T(t') \rangle = 2\alpha_d k_B T \delta_{ij} \delta(t - t')$. When the pinning is sufficiently strong, the system forms a topologically disordered state even at zero drive. After initialization, we set \mathbf{F}^T to zero and apply a uniform driving force $\mathbf{F}^D = F_D \hat{\mathbf{x}}$ on all the particles in the x -direction. To study the rate dependence, we increase the drive in increments of $\delta F_D = 0.002$ and wait for τ_q simulation time steps between increments. We stop the sweep at a particular maximum value of F_D , and we take $\tau_q = 5$ to 10000. For most of this work, we set $F_p = 1.0$ so that dynamical ordering near a drive of $F_D = 1.4$, and we study the defect densities near $F_D = 1.8$, above the dynamic reordering transition. For slow sweep rates or large values of τ_q , the system exhibits pinned, plastic, and dynamically ordered phases, with a critical depinning force F_c marking the transition from pinned to plastic flow, while the dynamical ordering force F_{cr} is defined as the drive at which the system dynamically orders into a moving

smectic or moving crystal. We pass across F_{cr} at different drive sweep rates and count the number of topological defects for a fixed value of F_D on the ordered side of F_{cr} . For small τ_q , more defects are present, and the KZ scenario predicts that the fraction of topological defects will scale as a power law with the quench rate. The vortices obey the same equation of motion as the skyrmions but have $\alpha_m = 0$, giving $\theta_{sk}^{\text{int}} = 0^\circ$.

III. RESULTS

In Fig. 1(a), we show a Voronoi plot of the vortex positions in a system with $F_p = 1.0$ at a drive of $F_D = 0.4$. In this case, the system is strictly overdamped with $\theta_{sk}^{\text{int}} = 0^\circ$, and the drive is increased from $F_D = 0$ to $F_D = 3.5$ in increments of $\delta F = 0.002$ with a waiting time of $\tau_q = 1000$ simulation time steps at each increment for a total time of $\tau = 1.75 \times 10^6$ simulation time steps. At this value of F_p , the system forms a disordered state when $F_D = 0$. At $F_D = 0.4$, the system has depinned and the particles are undergoing plastic flow in a fluid-like state. Figure 1(b) shows that the corresponding structure factor $S(\mathbf{k})$ has a ring signature indicative of disorder.

At higher drives, the system dynamically orders into a moving smectic, as illustrated in Fig. 1(c) at $F_D = 1.8$, where most of the particles form 1D chains and the topological defects are aligned in the direction of the drive. The corresponding $S(\mathbf{k})$ in Fig. 1(d) has the two pronounced peaks expected for a smectic structure. For slower quench rates, the system becomes more strongly ordered. Figure 1(e,f) shows the Voronoi and $S(\mathbf{k})$ plots for the same drive of $F_D = 1.8$ in a system with a finite Magnus force appropriate for skyrmions, with $\alpha_m = 0.8$, $\alpha_d = 0.6$, and $\theta_{sk}^{\text{int}} = 53.1^\circ$. In this case, near depinning the system is still disordered and has the same features shown in Fig. 1(a,b), but at high drives, the system becomes more strongly ordered and develops six peaks in $S(\mathbf{k})$, as shown Fig. 1(f), indicative of a moving crystal. This demonstrates that the nature of the driven ordered state in skyrmions is different from that of the vortices.

In Fig. 2 we plot the fraction P_6 of particles with six neighbors for the vortices and skyrmions from Fig. 1. Here $P_6 = N_v^{-1} \sum_i \delta(z_i - 6)$ where z_i is the coordination number of particle i obtained from the Voronoi construction. There is a critical drive F_{cr} at which the system shows an increase in order, indicative of the dynamic ordering transition. For the vortices, the increase in P_6 corresponding to F_{cr} falls at a lower drive value compared to the skyrmions, and the saturation value of P_6 is also lower for the vortices than for the skyrmions. The ordered state for the vortices is the moving smectic illustrated in Fig. 1(c,d), where the dislocations are locked in 1D channels and cannot climb. In contrast, for the skyrmion case, the system forms a moving crystal and the defects are able to climb, leading to the emergence of a more ordered state. This further underscores the fact

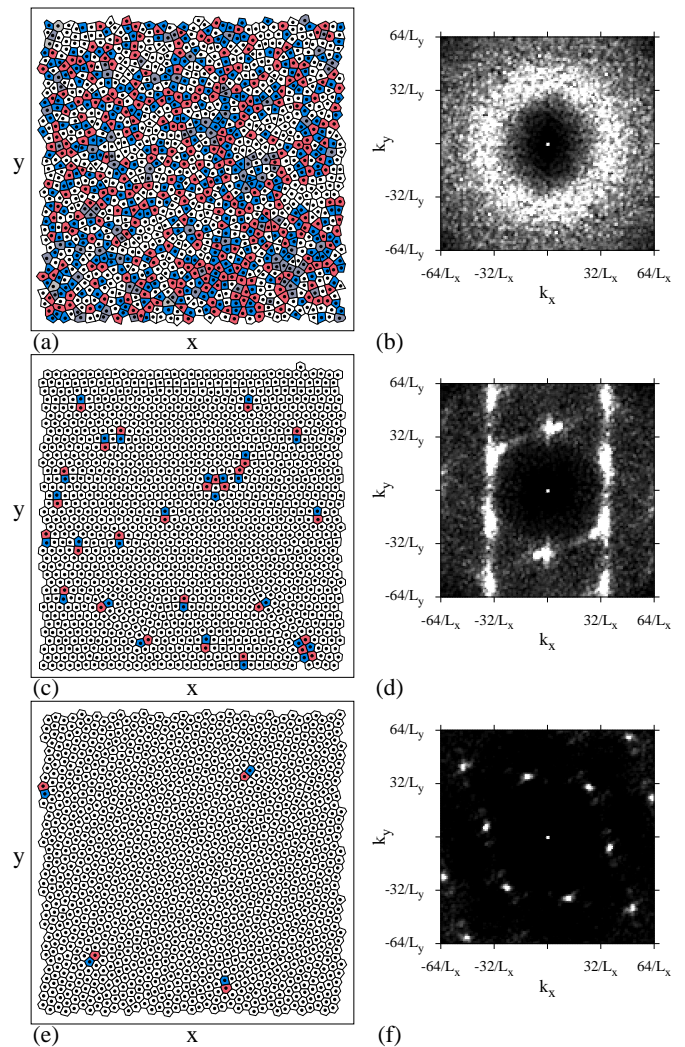


FIG. 1: (a,c,d) Voronoi construction for particles driven over quenched disorder with $F_p = 1.0$ at a waiting time of $\tau_q = 1000$. Polygons are colored according to coordination number: blue, five; white, six; red, seven; gray, all other values. (b,d,f) The corresponding structure factor $S(\mathbf{k})$. (a,b) The vortex case with $\theta_{sk}^{\text{int}} = 0^\circ$ at $F_D = 0.4$ where the system is topologically disordered. $S(\mathbf{k})$ has a ring structure. (c,d) The vortex case at $F_D = 1.8$, where the system forms a moving smectic and $S(\mathbf{k})$ develops two distinct peaks. (e,f) The skyrmion case with $\theta_{sk}^{\text{int}} = 53.1^\circ$ at $F_D = 1.8$ where the system forms a more isotropic crystal and $S(\mathbf{k})$ has an isotropic structure.

that the dynamically reordered states for the skyrmions and the vortices are different.

In Fig. 3(a), we plot $\langle V_x \rangle$ and $\langle V_y \rangle$, the velocities parallel and perpendicular to the driving direction, respectively, versus F_D for the same skyrmion system from Fig. 1(e,f) but for a quench rate that is ten times lower, $\tau_q = 10000$. Here there is a nonlinear regime near depinning, and at high drives, the velocity curves become linear. Figure 3(b) shows the absolute value of the measured skyrmion Hall angle, $\theta_{sk} = |\arctan(\langle V_y \rangle / \langle V_x \rangle)|$, which

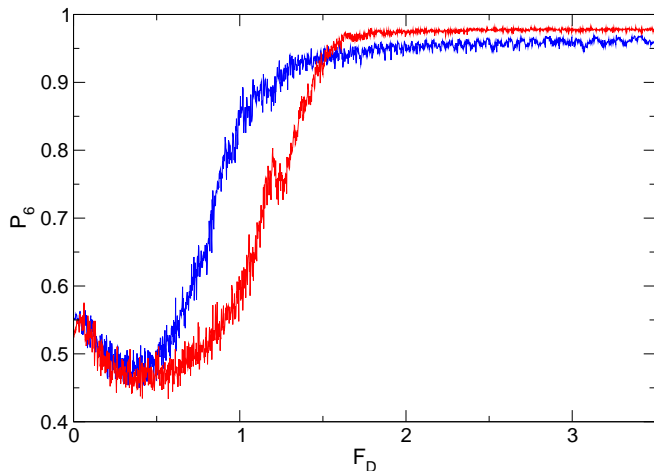


FIG. 2: The fraction P_6 of sixfold-coordinated particles vs F_D for the vortices with $\theta_{sk}^{\text{int}} = 0^\circ$ (blue) and skyrmions with $\theta_{sk}^{\text{int}} = 53.1^\circ$ (red) for the system from Fig. 1 with $F_p = 1.0$ and $\tau_q = 1000$. The skyrmions develop a larger amount of order at high drives.

starts off at zero in the pinned phase and increases linearly with increasing F_D before saturating at high drives to a value close to the intrinsic skyrmion Hall angle θ_{sk}^{int} . The velocity dependence of the skyrmion Hall angle has been studied previously in simulations^{35,37} and observed in experiments⁶⁹⁻⁷². The plot of P_6 versus F_D in Fig. 3(d) shows that P_6 is low in the plastic flow regime where θ_{sk} is increasing, but that a dynamical ordering transition occurs for $F_D > 1.325$ and the system orders into a mostly crystalline state with $P_6 \approx 0.98$. The skyrmion Hall angle is close to its intrinsic value when the system is on the ordered side of the transition.

Now that we have established the range of drives for which the system is ordered, we can sweep through the ordering transition at different rates and count the defects. Figure 4 shows P_6 versus F_D over the range $F_D = 0$ to $F_D = 3.5$ for quench times of $\tau_q = 10, 20, 40, 70, 100, 1000$, and 4000 , where the case of $\tau_q = 10000$ was already shown in Fig. 3. The quench times correspond to total simulation times of $10^3 \tau_q$. When $F_D > 1.3$, the system becomes more ordered as the value of τ_q increases. In Fig. 5 we plot the Voronoi constructions at $F_D = 1.8$ for $\tau_q = 10, 40, 100$, and 4000 , showing that for a given drive, fewer defects become trapped at lower quench rates.

In Fig. 6 we plot the fraction of defects, $P_d = 1 - P_6$, versus τ_d for both vortices and skyrmions from the system in Fig. 4 at a drive of $F_D = 1.8$. The lines are fits to $P_d \propto \tau_q^{-\beta}$ with $\beta = 0.5$ for the skyrmions and $\beta = 0.36$ for the vortices. The steeper slope for the skyrmion case is a reflection of the fact that the skyrmions can order more effectively than the vortices. Previous simulations³⁸ of the KZ scenario for vortices gave a value of $\beta \approx 0.385$, and it was argued that this was close to the value $\beta = 0.401$ expected for $1 + 1$ directed percolation since the vortices form 1D chains in the mov-

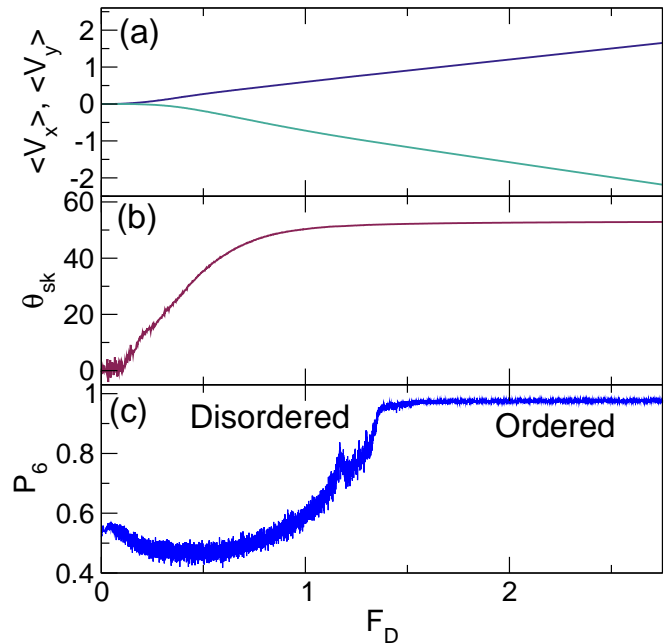


FIG. 3: Average velocities $\langle V_x \rangle$ (in the driving direction, blue) and $\langle V_y \rangle$ (perpendicular to the driving direction, green) vs F_D for the skyrmion system in Fig. 1(e,f) with $F_p = 1.0$ and $\theta_{sk}^{\text{int}} = 53.1^\circ$ but for a quench rate that is 10 times lower, $\tau_q = 10000$. (b) The corresponding absolute value of the measured Hall angle, $\theta_{sk} = |\arctan(\langle V_y \rangle / \langle V_x \rangle)|$, vs F_D . (c) P_6 vs F_D showing the disordered and ordered regimes on either side of the dynamical reordering transition.

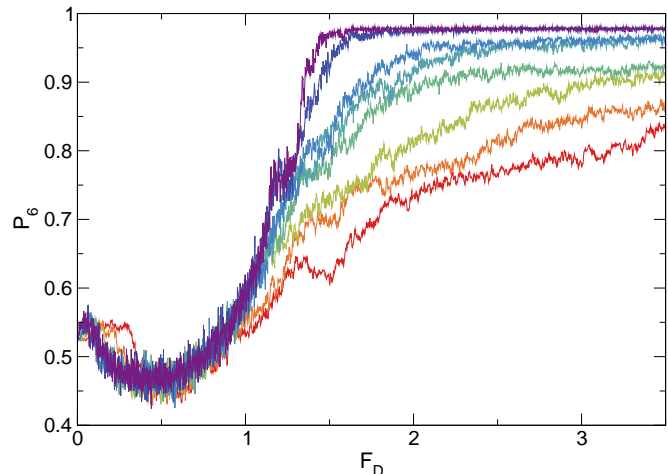


FIG. 4: P_6 vs F_D for the skyrmion system from Fig. 3 with $F_p = 1.0$ and $\theta_{sk}^{\text{int}} = 53.1^\circ$ over the range $F_D = 0$ to $F_D = 3.5$ for quench times of $\tau_q = 5$ (red), 10 (orange), 20 (light green), 40 (dark green), 70 (light blue), 100 (medium blue), 1000 (dark blue), and 4000 (purple). The curve for $\tau_q = 10000$ was already shown in Fig. 3. The quench times correspond to a total time of $10^3 \tau_q$.

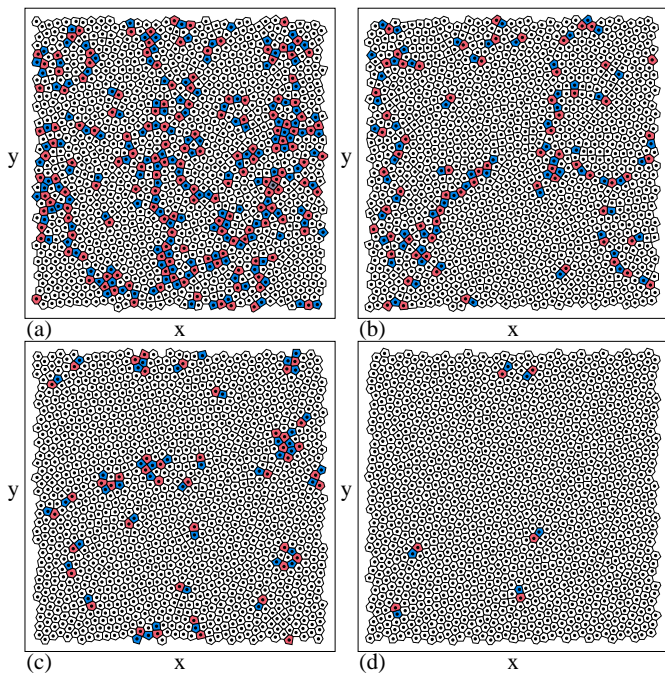


FIG. 5: The Voronoi construction at $F_D = 1.8$ for $\tau_q =$ (a) 10, (b) 40, (c) 100, and (d) 4000 for the skyrmion system in Fig. 4 with $F_p = 1.0$ and $\theta_{sk}^{\text{int}} = 53.1^\circ$.

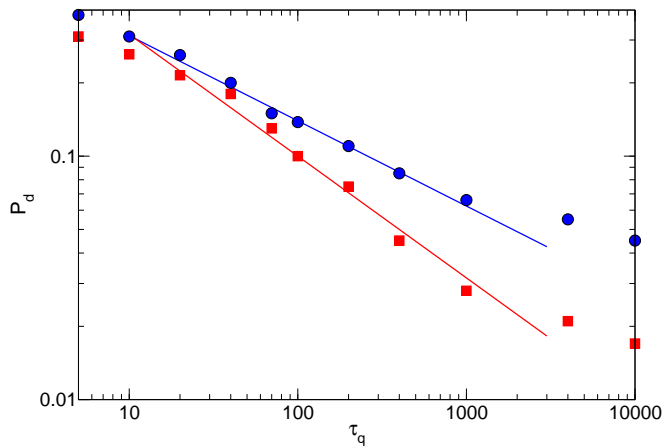


FIG. 6: The fraction of topological defects $P_d = 1 - P_6$ vs τ_q for the system from Fig. 4 with $F_p = 1.0$ at $F_D = 1.8$ for vortices with $\theta_{sk}^{\text{int}} = 0^\circ$ (blue) and skyrmions with $\theta_{sk}^{\text{int}} = 53.1^\circ$ (red). Lines indicate power law fits to $P_d \propto \tau_q^{-\beta}$, with $\beta = 0.36$ for the vortices (blue) and $\beta = 0.5$ for the skyrmions (red).

ing smectic state. The KZ scenario predicts that across a second-order phase transition, $\beta = (D - d)\nu/(1 + z\nu)$, which gives $\beta = 2/3$ for the 2D Ising model and $\beta = 0.6$ for 2D directed percolation^{38,43}, both of which are higher values than what we observe for the vortices and the skyrmions. Additionally, for very fast quenches in the skyrmion case, the fits give even lower values of β , which argues against the system being in the 2D Ising univer-

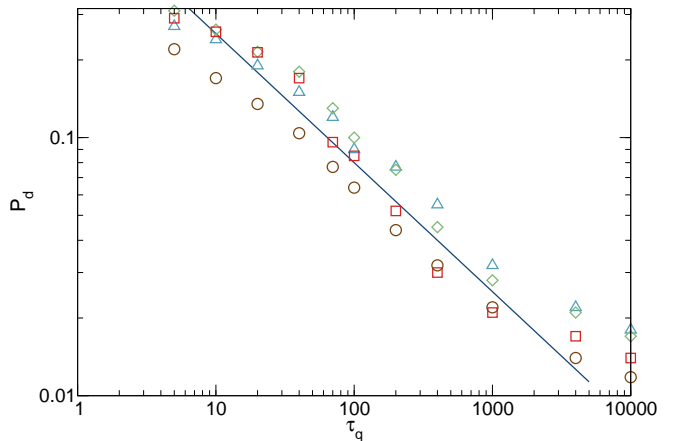


FIG. 7: P_d vs τ_q for the skyrmion system from Fig. 6 with $\theta_{sk}^{\text{int}} = 53.1^\circ$ for varied $F_p = 1.4$ (blue triangles), 1.0 (green diamonds), 0.7 (red squares), and 0.4 (brown circles). The defect densities are measured at a drive of $F_D = 1.2F_{cr}$ where F_{cr} is the critical dynamic reordering force. The solid line is a power law fit to $P_d \propto \tau_q^{-\beta}$ with exponent $\beta = 0.5$.

sality class. This suggests that although the behavior of the skyrmions is more 2D in character than that of the vortices, it is neither 2D directed percolation nor Ising-like. An exponent of $\beta = 1/2$ was obtained from quenches of a 2D artificial spin ice system⁵⁶, and it was argued that in that system, the dynamics is dominated by coarsening of the defects through the quench, leading to the formation of domain walls surrounding regions of size R . As a function of time, R increases⁷⁹ according to $R(t) = t^{1/2}$, and therefore the number of defects decreases with time as $1/R(t)$. In the skyrmion system, we find that some of the topological defects form domain walls, as illustrated in Fig. 5(b). In our simulations, once the skyrmion system is on the ordered side of the transition with $F_D > F_{cr}$, the topological defects interact strongly with each other and can annihilate through a coarsening process. As a result, different sweep rates τ_q give access to different portions of the coarsening process and produce exponents associated with coarsening. For the vortex system where the particles form 1D chains, the defects remain trapped in the chains and cannot climb, reducing the amount of coarsening that occurs and allowing a greater number of topological defects to survive on the ordered side of the transition, as shown in Fig. 2(b). We cannot rule out the possibility that the skyrmion system could fall in some other universality class or that the coarsening might compete with the critical dynamics.

In Fig. 7, we plot P_d versus τ_q for the skyrmion system with $\theta_{sk}^{\text{int}} = 53.1^\circ$ from Fig. 6 at varied pinning strengths of $F_p = 1.4, 1.0, 0.7$, and 0.4. The solid line is a power law fit with exponent $\beta = 0.5$. In this case, we examine the defect densities at $F_D = 1.2F_{cr}$ since the value of the critical reordering force F_{cr} varies as a function of F_p and the ratio α_m/α_d . In Fig. 8(a) we plot P_d versus τ_q for the same system at $F_p = 1.0$ but for varied Magnus

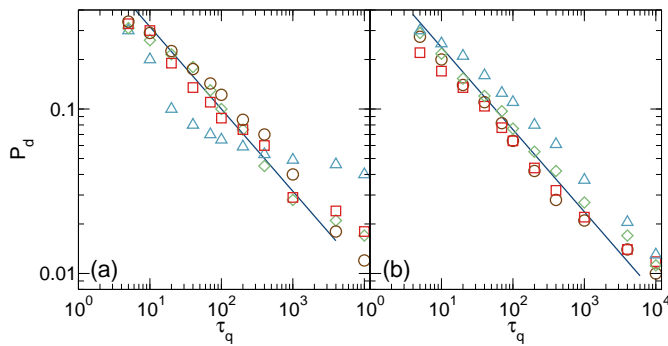


FIG. 8: P_d vs τ_q for the skyrmion system from Fig. 6 for varied $\theta_{sk}^{\text{int}} = 84.26^\circ$ (blue triangles), 53.1° (green diamonds), 37.95° (red squares), and 23.58° (brown circles). The defect densities are measured at $F_D = 1.2F_{cr}$. (a) $F_p = 1.0$. (b) $F_p = 0.4$. The solid lines are power law fits to $P_d \propto \tau_q^{-\beta}$ with $\beta = 0.5$.

force contributions giving $\theta_{sk}^{\text{int}} = 84.26^\circ$, 53.1° , 37.95° , and 23.58° . The solid line is a power law fit with $\beta = 0.5$. When $\theta = 84.26^\circ$, we observe significant deviations from the power law; however, in this case, α_m is ten times larger than α_d , so the dynamics are heavily dominated by gyrotropic motion. For the smaller skyrmion Hall angles, the exponents become more robust, and these smaller values of θ_{sk}^{int} are well within the range of what has been observed experimentally. Figure 8(b) shows the same variation of P_d versus τ_q with skyrmion Hall angle in a system with weaker pinning of $F_p = 0.4$. In general, we find that for skyrmion Hall angles greater than 10° , the system dynamically orders into an isotropic crystal and exhibits a scaling exponent close to $\beta = 0.5$, while for smaller skyrmion Hall angles (not shown), the system forms a moving smectic and β decreases toward the value obtained for vortices with $\theta_{sk}^{\text{int}} = 0^\circ$.

IV. INSTANTANEOUS QUENCHES

Another method for examining the behavior of the defects on the ordered side of the transition is to perform instantaneous quenches starting from a drive well below the critical ordering transition drive F_{cr} , where the system is topologically disordered. We instantaneously increase the drive to a value above F_{cr} and measure the time-dependent decay of the defect population. We specifically consider the system from Fig. 2 with $F_p = 1.0$, where the vortices with $\theta_{sk}^{\text{int}} = 0^\circ$ form a dynamically ordered smectic state but the skyrmions with $\theta_{sk}^{\text{int}} = 53.1^\circ$ form a dynamically ordered crystal, and we instantly change the driving from $F_D = 0.5$ to $F_D = 1.7$. The ordering transition for the skyrmions occurs near $F_{cr} = 1.325$.

The plot of P_d versus simulation time in Figure 9 for both vortices and skyrmions shows that there is an extended regime in which the population of defects continues to decrease for the skyrmion system, indicative of

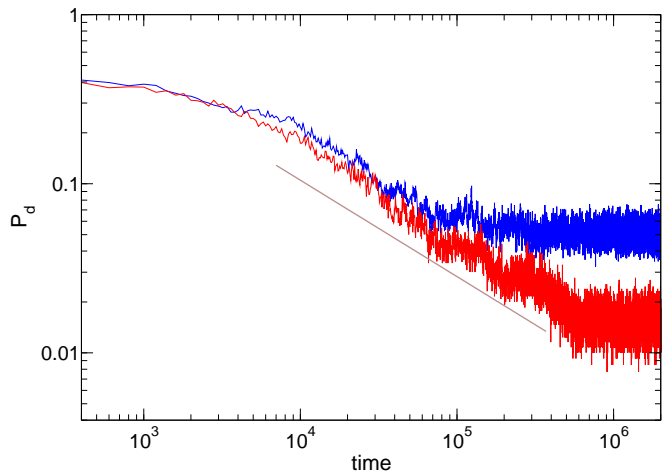


FIG. 9: The time dependence of the defect population P_d in simulation time units after an instantaneous quench from $F_D = 0.5$ to $F_D = 1.7$ for vortices with $\theta_{sk}^{\text{int}} = 0^\circ$ (blue) and skyrmions with $\theta_{sk}^{\text{int}} = 53.1^\circ$ (red) in a sample with $F_p = 1.0$. The defect density saturates at shorter times for the vortices than for the skyrmions. The solid line is a fit to $P_d \propto t^{-\alpha}$ with $\alpha = 0.57$.

coarsening, while in the vortex system the defect population rapidly saturates. The solid line is a power law fit to $P_d \propto t^{-\alpha}$ with $\alpha = 0.57$. This exponent is close to the value $\beta = 0.5$ obtained in Fig. 6 as a function of τ_q for finite rate quenches in the skyrmion system, suggesting that coarsening on the ordered side of the transition is occurring more strongly for the skyrmions than for the vortices. This could be due to the fact that the skyrmions form a more isotropic structure that allows both climb and glide of the defects, while the vortices form a smectic structure containing trapped defects that cannot annihilate. Generally, for any value of F_D in instantaneous quenches above the ordering drive, the skyrmions show an extended regime of coarsening compared to the vortices and reach a lower saturated value of P_d .

In Fig. 10 we plot P_d versus time for the skyrmion system from Fig. 9 for quenches from $F_D = 0.5$ to different final values of F_D . For final values of $F_D = 1.0$ and 1.2 , which are below the critical ordering drive F_{cr} , the defect populations show little change since the system remains in the disordered phase. For a final value of $F_D = 1.325$, which is just above the ordering transition, coarsening extends out to long times and can be described by a power law $P_d \propto t^{-\alpha}$ with $\alpha = 0.5$, as indicated by the dashed line. For a final value of $F_D = 1.7$, there is a similar extended range of coarsening, as also shown in Fig. 9. At a final value of $F_D = 2.0$, we start to see some deviations and there is a sharp jump down in the defect density at later times. In an isotropic driven system with quenched disorder, the particles can be regarded as experiencing an effective shaking temperature¹⁷ T_{eff} produced by the pinning, where $T_{\text{eff}} \propto 1/F_D$. As the final drive value increases, this effective temperature decreases and the

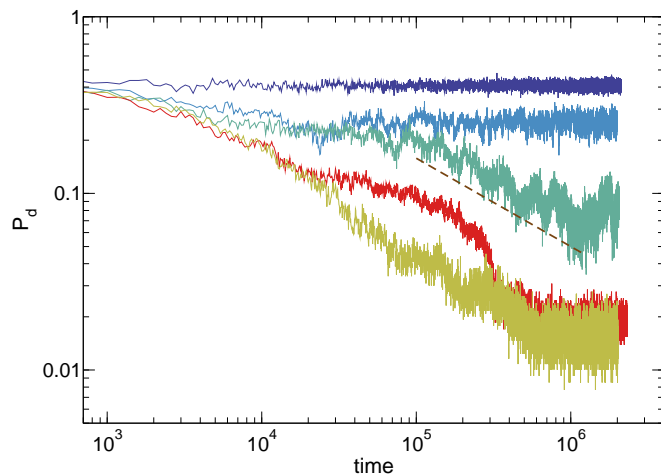


FIG. 10: The time dependence of P_d in simulation time units for the skyrmion system from Fig. 9 with $\theta_{sk}^{\text{int}} = 53.1^\circ$ and $F_p = 1.0$ after an instantaneous quench from $F_D = 0.5$ to $F_D = 1.0$ (dark blue), 1.2 (light blue), 1.325 (dark green), 1.7 (light green), and 2.0 (red). The dashed line is a power law fit to $P_d \propto t^{-\alpha}$ with exponent $\alpha = 0.5$.

amount of activated defect hopping is reduced, leading to a reduction in the amount of coarsening that occurs.

V. DISCUSSION AND SUMMARY

We have examined the topological defect populations upon passing through a nonequilibrium phase transition from a disordered plastic flow state to a two dimensional ordered or partially ordered moving state for vortices and skyrmions as a function of quench rate through the transition. In the overdamped vortex system, which as shown in previous work forms a moving smectic on the ordered side of the transition, the defect density varies as $P_d \propto \tau_q^{-\beta}$ with $\beta \approx 0.36$. It has been argued that this is a result of the fact that the reordering transition is an absorbing phase transition in the $1+1$ directed percolation universality class since the moving state forms 1D chains. Similar exponents were obtained in both simulations³⁸

and experiments³⁹. For the case of skyrmions where there is a nondissipative Magnus term, the ordered system forms a more isotropic moving crystal rather than a smectic state. In general, we find that the skyrmions can reach a much more ordered state than the vortices and that for the skyrmions, $\beta \approx 0.5$. This suggests that the dynamical ordering transition for the skyrmions falls into a different universality class than that of the vortices. We also argue that coarsening may be occurring for the skyrmions on the ordered side of the transition and that the difference in the skyrmion and vortex exponents could be the result of coarsening dynamics. To test this, we performed instantaneous quenches across the transition and found a similar decay in the defect populations for vortices and skyrmions at short times; however, at longer times, the defect population saturates much sooner and at a higher level for the vortices as the defects become trapped in the smectic structure, while for skyrmions the system continues to coarsen for a much longer time. For the skyrmions, the defect population after an instantaneous quench decays as a power law with an exponent in the range of $\alpha = 0.5$ to 0.57 . Our results suggest that the Kibble-Zurek scenario can be applied to nonequilibrium phase transitions in driven systems with quenched disorder, where depending on the nature of the ordered state, different scaling behavior can appear. For skyrmions, the dynamics may reflect coarsening rather than a critical scaling due to the ability of defects to annihilate even during the quench. It would be interesting to apply the Kibble-Zurek scenario to other driven systems with quenched disorder, such as those with periodic substrates, to three dimensional or layered systems, and also to explore different types of driving protocols.

Acknowledgments

This work was supported by the US Department of Energy through the Los Alamos National Laboratory. Los Alamos National Laboratory is operated by Triad National Security, LLC, for the National Nuclear Security Administration of the U. S. Department of Energy (Contract No. 892333218NCA000001).

¹ H. E. Stanley, *Introduction to Phase Transitions and Critical Phenomena* (Clarendon Press, Oxford, 1971).

² N. Goldenfeld, *Lectures on Phase Transitions and the Renormalization Group* (Westview Press, Oxford, 1992).

³ H. Hinrichsen, *Adv. Phys.* **49**, 815 (2000).

⁴ K. A. Takeuchi, M. Kuroda, H. Chaté, and M. Sano, *Phys. Rev. Lett.* **99**, 234503 (2007).

⁵ H.-Y. Shih, T.-L. Hsieh, and N. Goldenfeld, *Nature Phys.* **12**, 245 (2016).

⁶ M. Sano and K. Tamai, *Nature Phys.* **12**, 249 (2016).

⁷ G. Lemoult, L. Shi, K. Avila, S. V. Jalikop, M. Avila, and B. Hof, *Nature Phys.* **12**, 254 (2016).

⁸ L. Corte, P. M. Chaikin, J. P. Gollub, and D. J. Pine, *Nature Phys.* **4**, 420 (2008).

⁹ M. Fruchart, R. Hanai, P. B. Littlewood, and V. Vitelli, *Nature* **592**, 363 (2021).

¹⁰ D. S. Fisher, *Phys. Rep.* **301**, 113 (1998).

¹¹ Y. Fily, E. Olive, N. Di Scala, and J. C. Soret, *Phys. Rev. B* **82**, 134519 (2010).

¹² C. Reichhardt and C. J. O. Reichhardt, *Rep. Prog. Phys.* **80**, 026501 (2017).

¹³ T. Bohlein and C. Bechinger, *Phys. Rev. Lett.* **109**, 058301 (2012).

¹⁴ A. Vanossi, N. Manini, M. Urbakh, S. Zapperi, and

- E. Tosatti, *Rev. Mod. Phys.* **85**, 529 (2013).
- 15 G. Blatter, M. V. Feigel'man, V. B. Geshkenbein, A. I. Larkin, and V. M. Vinokur, *Rev. Mod. Phys.* **66**, 1125 (1994).
 - 16 S. Bhattacharya and M. J. Higgins, *Phys. Rev. Lett.* **70**, 2617 (1993).
 - 17 A. E. Koshelev and V. M. Vinokur, *Phys. Rev. Lett.* **73**, 3580 (1994).
 - 18 U. Yaron, P. L. Gammel, D. A. Huse, R. N. Kleiman, C. S. Oglesby, E. Bucher, B. Batlogg, D. J. Bishop, K. Mortensen, and K. N. Clausen, *Nature (London)* **376**, 753 (1995).
 - 19 M. C. Hellerqvist, D. Ephron, W. R. White, M. R. Beasley, and A. Kapitulnik, *Phys. Rev. Lett.* **76**, 4022 (1996).
 - 20 K. Moon, R. T. Scalettar, and G. T. Zimányi, *Phys. Rev. Lett.* **77**, 2778 (1996).
 - 21 L. Balents, M. C. Marchetti, and L. Radzihovsky, *Phys. Rev. B* **57**, 7705 (1998).
 - 22 P. Le Doussal and T. Giamarchi, *Phys. Rev. B* **57**, 11356 (1998).
 - 23 F. Pardo, F. de la Cruz, P. L. Gammel, E. Bucher, and D. J. Bishop, *Nature* **396**, 348 (1998).
 - 24 C. J. Olson, C. Reichhardt, and F. Nori, *Phys. Rev. Lett.* **81**, 3757 (1998).
 - 25 S. Maegochi, K. Ienaga, and S. Okuma, *Phys. Rev. Res.* **4**, 033085 (2022).
 - 26 A. C. Marley, M. J. Higgins, and S. Bhattacharya, *Phys. Rev. Lett.* **74**, 3029 (1995).
 - 27 S. Okuma, K. Kashiro, Y. Suzuki, and N. Kokubo, *Phys. Rev. B* **77**, 212505 (2008).
 - 28 P. Tierno, *Phys. Rev. Lett.* **109**, 198304 (2012).
 - 29 C. Reichhardt, C. J. Olson, N. Grønbech-Jensen, and F. Nori, *Phys. Rev. Lett.* **86**, 4354 (2001).
 - 30 J. Sun, J. Niu, Y. Li, Y. Liu, L. N. Pfeiffer, K. W. West, P. Wang, and X. Lin, *Fund. Res.* **2**, 178 (2022).
 - 31 C. Reichhardt, C. J. O. Reichhardt, I. Martin, and A. R. Bishop, *Phys. Rev. Lett.* **90**, 026401 (2003).
 - 32 H. J. Zhao, V. R. Misko, and F. M. Peeters, *Phys. Rev. E* **88**, 022914 (2013).
 - 33 E. Granato, J. A. P. Ramos, C. V. Achim, J. Lehtikoinen, S. C. Ying, T. Ala-Nissila, and K. R. Elder, *Phys. Rev. E* **84**, 031102 (2011).
 - 34 C. Sándor, A. Libál, C. Reichhardt, and C. J. Olson Reichhardt, *Phys. Rev. E* **95**, 032606 (2017).
 - 35 C. Reichhardt, D. Ray, and C. J. O. Reichhardt, *Phys. Rev. Lett.* **114**, 217202 (2015).
 - 36 W. Koshibae and N. Nagaosa, *Sci. Rep.* **8**, 6328 (2018).
 - 37 C. Reichhardt and C. J. O. Reichhardt, *Phys. Rev. B* **99**, 104418 (2019).
 - 38 C. J. O. Reichhardt, A. del Campo, and C. Reichhardt, *Commun. Phys.* **5**, 173 (2022).
 - 39 S. Maegochi, K. Ienaga, and S. Okuma, *Phys. Rev. Lett.* **129**, 227001 (2022).
 - 40 T. W. B. Kibble, *J. Phys. A: Math. Gen.* **9**, 1387 (1976).
 - 41 W. H. Zurek, *Nature (London)* **317**, 505 (1985).
 - 42 W. H. Zurek, *Phys. Rep.* **276**, 177 (1996).
 - 43 A. del Campo and W. H. Zurek, *Int. J. Mod. Phys. A* **29**, 1430018 (2014).
 - 44 M. J. Bowick, L. Chandar, E. A. Schiff, and A. M. Srivastava, *Science* **263**, 943 (1994).
 - 45 C. N. Weiler, T. W. Neely, D. R. Scherer, A. S. Bradley, M. J. Davis, and B. P. Anderson, *Nature (London)* **455**, 948 (2008).
 - 46 S. Ulm, J. Roßnagel, G. Jacob, C. Degüenther, S. T. Dawkins, U. G. Poschinger, R. Nigmatullin, A. Retzker, M. B. Plenio, F. Schmidt-Kaler, et al., *Nature Commun.* **4**, 2290 (2013).
 - 47 K. Pyka, J. Keller, H. L. Partner, R. Nigmatullin, T. Burgermeister, D. M. Meier, K. Kuhlmann, A. Retzker, M. B. Plenio, W. H. Zurek, et al., *Nature Commun.* **4**, 2291 (2013).
 - 48 S. Deutschländer, P. Dillmann, G. Maret, and P. Keim, *Proc. Natl. Acad. Sci. (USA)* **112**, 6925 (2015).
 - 49 A. Keesling, A. Omran, H. Levine, H. Bernien, H. Pichler, S. Choi, R. Samajdar, S. Schwartz, P. Silvi, S. Sachdev, et al., *Nature (London)* **568**, 207 (2019).
 - 50 S. Casado, W. González-Viñas, and H. Mancini, *Phys. Rev. E* **74**, 047101 (2006).
 - 51 A. Zamora, G. Dagvadorj, P. Comaron, I. Carusotto, N. P. Proukakis, and M. H. Szymańska, *Phys. Rev. Lett.* **125**, 095301 (2020).
 - 52 K. R. Elder, J. Viñals, and M. Grant, *Phys. Rev. Lett.* **68**, 3024 (1992).
 - 53 C. Harrison, D. H. Adamson, Z. Cheng, J. M. Sebastian, S. Sethuraman, D. A. Huse, R. A. Register, and P. M. Chaikin, *Science* **290**, 1558 (2000).
 - 54 H. Qian and G. F. Mazenko, *Phys. Rev. E* **67**, 036102 (2003).
 - 55 L. Purvis and M. Dennin, *Phys. Rev. Lett.* **86**, 5898 (2001).
 - 56 A. Libál, A. del Campo, C. Nisoli, C. Reichhardt, and C. J. O. Reichhardt, *Phys. Rev. Res.* **2**, 033433 (2020).
 - 57 S. Mühlbauer, B. Binz, F. Jonietz, C. Pfleiderer, A. Rosch, A. Neubauer, R. Georgii, and P. Böni, *Science* **323**, 915 (2009).
 - 58 X. Z. Yu, Y. Onose, N. Kanazawa, J. H. Park, J. H. Han, Y. Matsui, N. Nagaosa, and Y. Tokura, *Nature (London)* **465**, 901 (2010).
 - 59 N. Nagaosa and Y. Tokura, *Nature Nanotechnol.* **8**, 899 (2013).
 - 60 K. Everschor-Sitte, J. Masell, R. M. Reeve, and M. Kläui, *J. Appl. Phys.* **124**, 240901 (2018).
 - 61 C. Reichhardt, C. J. O. Reichhardt, and M. Milosevic, *Rev. Mod. Phys.* **94**, 035005 (2022).
 - 62 F. Jonietz, S. Mühlbauer, C. Pfleiderer, A. Neubauer, W. Münzer, A. Bauer, T. Adams, R. Georgii, P. Böni, R. A. Duine, et al., *Science* **330**, 1648 (2010).
 - 63 J. Zang, M. Mostovoy, J. H. Han, and N. Nagaosa, *Phys. Rev. Lett.* **107**, 136804 (2011).
 - 64 J. Iwasaki, M. Mochizuki, and N. Nagaosa, *Nature Commun.* **4**, 1463 (2013).
 - 65 S.-Z. Lin, C. Reichhardt, C. D. Batista, and A. Saxena, *Phys. Rev. Lett.* **110**, 207202 (2013).
 - 66 D. Liang, J. P. DeGrave, M. J. Stolt, Y. Tokura, and S. Jin, *Nature Commun.* **6**, 8217 (2015).
 - 67 C. Reichhardt and C. J. O. Reichhardt, *New J. Phys.* **18**, 095005 (2016).
 - 68 D. Okuyama, M. Bleuel, J. S. White, Q. Ye, J. Krzywón, G. Nagy, Z. Q. Im, I. Živković, M. Bartkowiak, H. M. Rønnow, et al., *Commun. Phys.* **2**, 79 (2019).
 - 69 W. Jiang, X. Zhang, G. Yu, W. Zhang, X. Wang, M. B. Jungfleisch, J. E. Pearson, X. Cheng, O. Heinonen, K. L. Wang, et al., *Nature Phys.* **13**, 162 (2017).
 - 70 K. Litzius, I. Lemesh, B. Krüger, P. Bassirian, L. Caretta, K. Richter, F. Büttner, K. Sato, O. A. Tretiakov, J. Förster, et al., *Nature Phys.* **13**, 170 (2017).
 - 71 R. Juge, S.-G. Je, D. d. S. Chaves, L. D. Buda-Prejbeanu, J. Peña Garcia, J. Nath, I. M. Miron, K. G. Rana, L. Aballe, M. Foerster, et al., *Phys. Rev. Applied* **12**,

- 044007 (2019).
- ⁷² K. Zeissler, S. Finizio, C. Barton, A. J. Huxtable, J. Massey, J. Raabe, A. V. Sadovnikov, S. A. Nikitov, R. Brearton, T. Hesjedal, et al., *Nature Commun.* **11**, 428 (2020).
- ⁷³ R. Brearton, L. A. Turnbull, J. A. T. Verezhak, G. Balakrishnan, P. D. Hatton, G. van der Laan, and T. Hesjedal, *Nature Commun.* **12**, 2723 (2021).
- ⁷⁴ S. A. Díaz, C. J. O. Reichhardt, D. P. Arovas, A. Saxena, and C. Reichhardt, *Phys. Rev. B* **96**, 085106 (2017).
- ⁷⁵ S.-Z. Lin, C. Reichhardt, C. D. Batista, and A. Saxena, *Phys. Rev. B* **87**, 214419 (2013).
- ⁷⁶ B. L. Brown, U. C. Täuber, and M. Pleimling, *Phys. Rev. B* **100**, 024410 (2019).
- ⁷⁷ N. P. Vizarim, J. C. B. Souza, C. J. O. Reichhardt, C. Reichhardt, M. V. Milošević, and P. A. Venegas, *Phys. Rev. B* **105**, 224409 (2022).
- ⁷⁸ Y. Ge, J. Rothörl, M. A. Brems, N. Kerber, R. Gruber, T. Dohi, M. Kläui, and P. Virnau, *Commun. Phys.* **6**, 30 (2023).
- ⁷⁹ P. C. Hohenberg and B. I. Halperin, *Rev. Mod. Phys.* **49**, 435 (1977).